Article:
Aboalhamayie, A. orcid.org/0000-0002-3934-5976, Ahmad, N., Zhang, Y. et al. (3 more authors) (2024) An experimental evaluation of thermophysical properties of colloidal suspension of carbon-rich fly ash microparticles and single-walled carbon nanotubes in Jet-A fuel and its impact on evaporation and burning rate. Fuel Processing Technology, 266. 108155. ISSN 0378-3820

https://doi.org/10.1016/j.fuproc.2024.108155

Fuel Processing Technology 266 (2024) 108155

Contents lists available at ScienceDirect

Fuel Processing Technology

journal homepage: www.elsevier.com/locate/fuproc

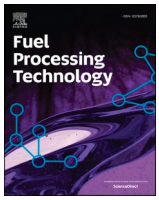

An experimental evaluation of thermophysical properties of colloidal suspension of carbon-rich fly ash microparticles and single-walled carbon nanotubes in Jet-A fuel and its impact on evaporation and burning rate

Ahmed Aboalhamayie [a,*], Nadeem Ahmad [b], Yang Zhang [a], Mohsen Ghamari [b], Numan Salah [c], Jameel Alshahrani [d]

[a] Department of Mechanical Engineering, The University of Sheffield, Sheffield S1 3JD, United Kingdom
[b] Department of Mechanical and Electrical Engineering, Wilkes University, Wilkes-Barre, PA 18766, USA
[c] Center of Nanotechnology, King Abdul Aziz University, Jeddah 21589, Saudi Arabia
[d] MA'ADEN, Riyadh 11537, Saudi Arabia

ARTICLE INFO

Keywords:
Carbon-rich fly ash (CFA)
Ignition delay
Single-walled carbon nanotube (SWCNT)
Evaporation rate
Surface tension
Thermal conductivity
Jet-A fuel

ABSTRACT

This study presents an experimental evaluation of the thermophysical properties of colloidal suspensions of carbon-rich fly ash microparticles (CFA) and single-walled carbon nanotubes (SWCNT) in Jet-A fuel, focusing on their impact on evaporation and burning rates. The research explores the effects of these carbon-based additives on key parameters such as thermal conductivity, viscosity, surface tension, evaporation rate, and combustion behavior. Utilizing a hybrid preparation method combining sonication and surfactants, stable colloidal suspensions were prepared for experimental analysis. The results demonstrate that both CFA and SWCNT enhance the thermal conductivity of Jet-A fuel, with SWCNT achieving a notable 13 % increase at a 1 wt% concentration, while CFA achieves an 8 % increase at a 3 wt% concentration. The study also reveals distinct trends in viscosity and surface tension, with SWCNT causing a significant non-linear increase in viscosity compared to CFA. In combustion experiments, the evaporation rates of CFA and SWCNT suspensions showed considerable improvement, with CFA demonstrating up to an 87 % increase at 1 wt% concentration. The study concludes with an analysis of ignition delay, highlighting the superior performance of SWCNT in reducing ignition time due to their high thermal conductivity and the presence of iron nanoparticles on their surface.

1. Introduction

During the combustion of heavy fuel or crude oil in boilers, oil droplets are subjected to intense heat and oxidation, leading to the depletion of the fuel. Concurrently, impurities such as sulfur, vanadium, and nickel undergo complex chemical transformations. These impurities react with gaseous hydrocarbons, resulting in the formation of particulates known as ash [1]. Approximately 3 kg of ash are generated per kiloliter of heavy fuel oil combusted [2], with about 90 % of this ash being fly ash, which is typically collected by electrostatic precipitators or cyclones for disposal or reuse [3]. Heavy Oil Fly Ash (HOFA) is composed of inorganic substances, including silicon dioxide (SiO_2), iron oxide (Fe_2O_3), aluminum oxide (Al_2O_3), and 70–80 % unburned carbon [4]. Salah et al. [5] have meticulously investigated the chemical composition of HOFA, revealing its unique porous structures. This material presents promising applications in the cement and concrete industry, contributing to environmentally sustainable construction practices [6]. Experimental investigations have explored the enhancement of epoxy resin by incorporating HOFA as a reinforcing agent. These studies have revealed significant improvements in tensile strength and have provided insights into the material's effects on thermal conductivity and diffusivity [7,8]. Additionally, HOFA has demonstrated efficacy as an anti-corrosion agent in steel structure coatings and treatments [9]. Detailed studies have elucidated the microscopic architecture of HOFA, emphasizing its potential as a lubricant additive in base oils [10]. Furthermore, HOFA has been employed in alkali metal ion batteries [11] and water treatment processes [12].

The incorporation of micro- and nano-sized particles into liquid fuels has been extensively researched, demonstrating enhancements in properties such as thermal conductivity [13]. The inclusion of carbon

* Corresponding author at: The University of Sheffield, Department of Mechanical Engineering, Sir Frederick Mappin Building, Sheffield S1 3JD, United Kingdom.
E-mail address: amaboalhamayie1@sheffield.ac.uk (A. Aboalhamayie).

https://doi.org/10.1016/j.fuproc.2024.108155
Received 13 September 2024; Received in revised form 3 November 2024; Accepted 5 November 2024
Available online 16 November 2024

materials, whether in nano or micron dimensions, has been shown to improve optical properties and combustion rates. For instance, Ghamari and Ratner's experimental studies have demonstrated enhanced combustion rates for graphene nanoplatelets (GNP), multi-walled carbon nanotubes (MWCNT), and activated carbon particles in Jet-A fuel [14]. Moreover, Aboalhamayie et al. have investigated the increased evaporation rates in Jet-A fuel, attributed to the enhanced thermal conductivity from added carbon nanomaterials [15]. Notably, the carbon content in the residue of heavy oil combustion, referred to as rich carbon fly ash, is analogous to that found in activated carbon nanomaterials used in previous studies such as [14,15]. Ziabakhsh and Shassemi [16] conducted a comprehensive study on the morphological structure of residues from combusted heavy fuel oil, identifying four types of residues influenced by temperature variations. Bui and Bui [17] examined the effect of a 0.5 % fly ash additive in various types of oil, comparing it to samples without the additive. Their findings highlighted the effectiveness of fly ash additives in mitigating the impact of temperature on oil viscosity. Chaudhari et al. [18] studied the addition of fly ash at mass fractions of 3 % and 6 % in diesel emulsion with water, experimentally demonstrating that fly ash functions as a combustion improver and emission reduction additive, enhancing efficiency and reducing NOx emissions.

Single-wall carbon nanotubes, renowned for their high thermal conductivity of 2000 W/m·K [19], serve as a comparative benchmark for heavy oil fly ash, especially since previous research has examined carbon nanoparticles (CNP), GNP, and MWCNT [14–16]. These intriguing parallels necessitate a comprehensive examination of HOFA's potential, particularly its influence on key research parameters such as stability of colloidal suspension, thermal conductivity, viscosity, surface tension, evaporation rate, combustion rate, and ignition delay.

2. Methods

2.1. Sample preparation

Two different types of carbon-based materials were used to prepare Micro/Nano fuel samples at different concentrations: Carbon Fly Ash (CFA), also known as Heavy Oil Fly Ash (HOFA), that was directly collected from the electrostatic precipitator (ESP) of the Rabigh IPP power plant, located in Rabigh on the coast of the Red Sea in western Saudi Arabia, and Single-Walled Carbon Nanotubes (SWCNT), that were purchased from Nanostructured and Amorphous Materials Inc. (Product ID 1246YJS). The elemental composition of CFA is presented in Table 1 while Table 2 summarizes the physical properties of both particles.

The dimension and morphology of micro and nanoparticles can affect the way they promote energy transfer mechanisms through colloidal fuels. For instance, particles with a larger specific surface area (SSA) are expected to be more efficient in transferring heat within the liquid fuel. The morphology and microscopic structure of SWCNT and CFA is shown in Fig. 1.

In conducting any successful measurement and experimental research on a Micro/Nano fuel type, preparing a stable colloidal suspension of micro and nanoparticles dispersed in the fuel is a key step. Measuring thermal conductivity, surface tension, and viscosity as thermophysical properties may take up to 30 min, and hence, it is necessary

Table 1
Chemical composition of Carbon Fly Ash microparticles (data collected from ref. [5]).

Element	Weight%
C	84.4
O	8.39
S	4.51
Fe	2.53
V	0.17

Table 2
Physical properties of carbon particles (SSA: specific surface area; OD: outer diameter; ID: inner diameter).

Particle Type	CFA	SWCNT
Size (μm and nm)	30 μm	OD 1–2 nm; length 1–3 μm
Bulk Density (g/cm^3)	1.07	0.36–0.42
SSA (m^2/g)	1.8 [7]	> 340

to prepare suspensions that will remain stable throughout the whole duration of the experimental measurement. Magnetic stirring, sonication, and adding surfactants as stabilizer chemical agents are common techniques to prevent or slow down particle agglomeration. Combining these methods has been reported to extend the stability of Micro/Nano fluids [20]. As a result, a hybrid method, also known in the field as two-step approach, employing a surfactant and agitation through sonication, was specifically adopted as follows: initially, a 3 % (by weight) solution of a nonionic surfactant (Sorbitan Monooleate, known as Span 80) in Jet-A fuel was prepared on a magnet stirrer for 30 min. Span 80 has a hydrophilic-lipophilic balance of 4.3 ± 1.0, and easily dissolves in base fuel. While still stirring, the particles were added to the solution at different concentrations and were allowed to mix for another 10 min until a visually homogeneous mixture was obtained. To improve the stability of nanofuel and prevent the quick agglomeration of particles, prepared samples were sonicated using an ultrasonic bath (Elmasonic S10H). Only 20 mL of each sample was prepared, and a power setting of only 30 % on the sonication bath was used. To achieve an optimum micro and nanofuel preparation technique, various sonication times were tried until it was determined that intermittent sonication for 45 min can yield colloids that will not go through phase separation for at least 20 to 60 min after the sonication, as shown in Fig. 3. Two approaches were employed to evaluate the stability of colloidal suspensions: one using an experimental apparatus and the other through visual inspection with a flashlight. In Fig. 2 The experimental apparatus, meticulously designed in the lab, consists of an infrared (IR) laser, an IR receiver (detector), a linear actuator, a micro slider, a microcontroller, and a sample holder. Both the IR laser and receiver are powered by a 3-V source. The linear actuator is connected to the micro slider through a fixed pin support, allowing for precise movement and ensuring optimal alignment for accurate detection. The apparatus is configured so that the sample is centrally positioned between the IR laser and the receiver. When activated, the IR laser emits a beam in a parallel direction directly aimed at the IR receiver positioned on the opposite side.

As the colloidal suspension in the fuel sample begins to settle and the medium becomes sufficiently clear, the IR laser beam can pass through the glass laboratory setup. This unobstructed passage is detected by the IR receiver, which registers a signal of '0,' indicating clear detection. Conversely, if the beam is blocked by suspended particles, the receiver continues to register '1,' reflecting an uninterrupted signal or no obstruction in the laser's path. It is worth noting that the system is equipped with four laser-IR receiver pairs, strategically positioned to detect any phase separation occurring at different levels—whether in the middle or at the bottom of the sample. This methodology offers a powerful approach to understanding the stability duration of each colloidal suspension, particularly when examined under conditions such as those in a thermal conductivity apparatus. The black color of carbon nano and micro particles used in this study results in suspensions that completely block light right after sonication as showing in Fig. 3. However, as the particles agglomerate, aggregates are formed and begin to settle at the bottom of the container under the effect of gravity. As a result, the suspension begins to turn murky at the liquid surface and gradually downward. It is noteworthy that due to their morphology and large specific surface area, SWCNT are more susceptible to entangling around each other and form agglomerates.

Conversely, Fig. 4 presents the averaged results of three experiments conducted for each particle concentration using the experimental

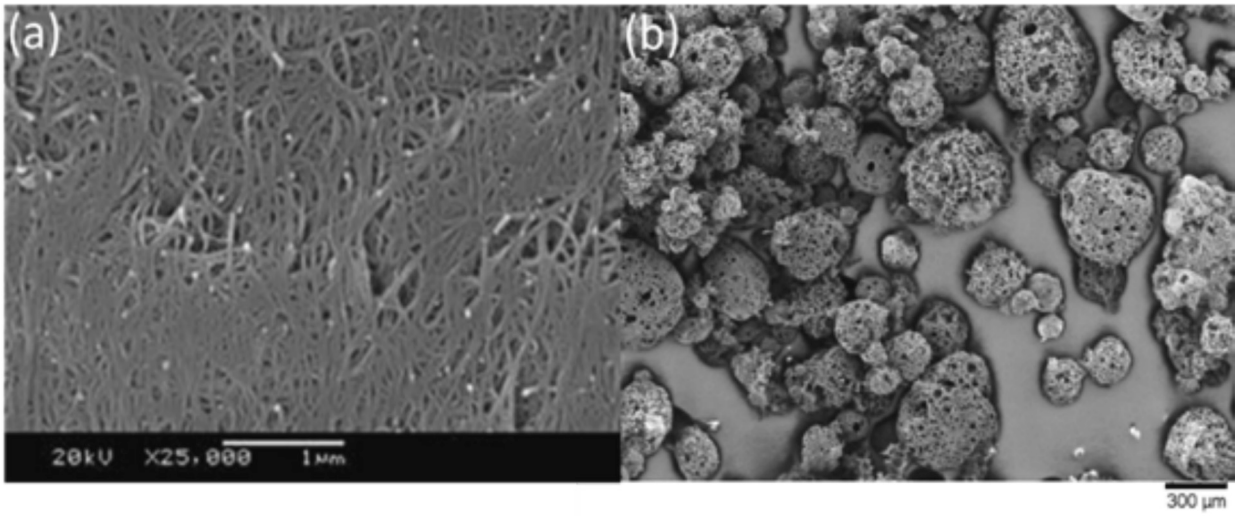

Fig. 1. Scanning electron microscope (SEM) images at various magnifications: (a) single walled carbon nanotubes (courtesy of Nanostructures & Amorphous Materials, inc.) and (b) carbon rich fly ash.

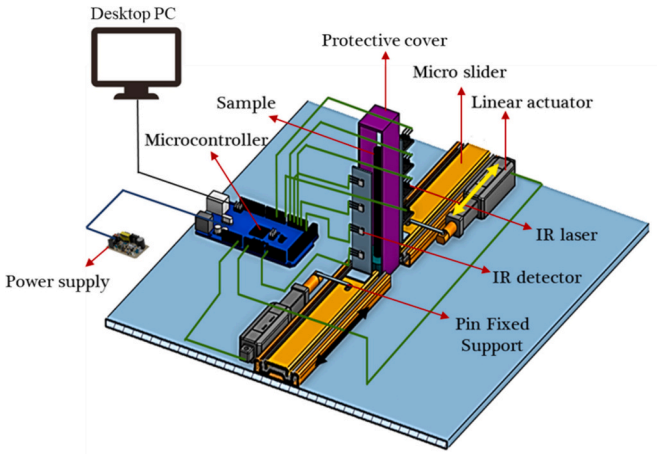

Fig. 2. Schematic of Micro/Nano fluid stability experimental apparatus.

apparatus shown in Fig. 2. CFA suspensions show varying levels of stability: 0.25 % and 0.5 % suspensions remain stable for one hour. At 1 %, visual stability persists for 55 min, diminishing to 45 min at 2 %, and

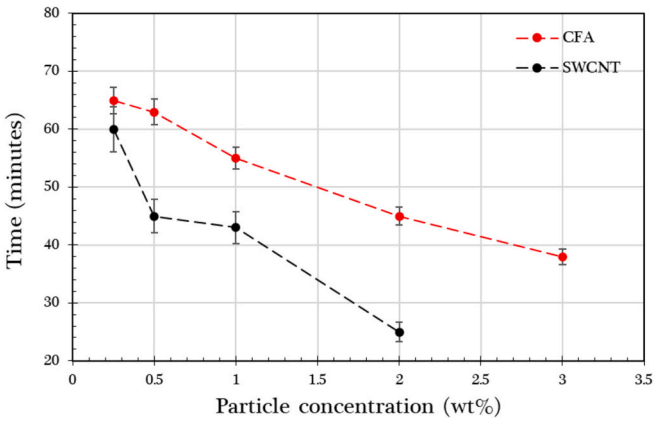

Fig. 4. Stability time in (minutes) of CFA and SWCNT colloidal suspension as a function of particle concentration.

Fig. 3. Stability of 0.25 % Jet-A fuel +CFA Nano particles colloidal suspension right after preparation at interval of time after preparation 0, 45, 60 min, and by IR detection apparatus.

further to 38 min at 3 %. Conversely, colloidal suspensions of SWCNT display different durations of stability: 0.25 % sustains stability for one hour, 0.5–1 % for 45 min, and 2 % for 25 min. Recognizing the duration of stability is paramount to mitigating potential errors arising from phase separation during measurements of physical properties. In particular, thermal conductivity measurement takes nearly 20 min, and as such it is imperative for the prepared colloidal suspension to maintain stability, thereby averting phase separation, for a minimum duration of 20 min.

2.2. Thermo-physical property measurement (conductivity, surface tension, and viscosity)

The thermal conductivity of colloidal fuels was determined using the Hilton H470 apparatus, as shown in Fig. 5, and according to the following concept: A thin radial layer of the fuel sample is subjected to heat flow supplied by a thermal resistance, connected to a transformer, and allowing for a constant heat rate by adjusting the voltage. To maintain equilibrium and facilitate heat dissipation, a continuous flow of cold water at a rate of 3 L per minute circulates through a cooling jacket surrounding the fuel sample. Two Type-K thermocouples are utilized to measure the temperature difference across the thin layer of fuel, and the thermal conductivity is then determined by applying Fourier's law of heat conduction. The assessment of thermal conductivity involves particles at concentrations ranging from 0.25 % to 3 %. For each concentration, the liquid samples are subjected to three distinct heat fluxes by applying voltages of 100, 120, and 140 V. Temperature measurements are taken on both sides of the liquid sheet, and once equilibrium is reached, the average of these temperatures is recorded as the mean temperature of the fuel sample.

When it comes to liquid fuel combustion, atomization is a critical step to generate enough surface area. This is done by spraying liquid fuel and forming small droplets. Viscosity and surface tension are two key physical properties affecting spray characteristics and droplet formation. In particular, surface tension determines the droplet size. It is also due to instabilities caused by surface tension that liquid jets or sheet break up into droplets. Similarly, liquid viscosity impacts droplet size and its formation by affecting the energy required to break the liquids. In general, high viscosity and surface tension result in more spherical droplets leading to lower evaporation rate due to smaller surface area. Higher viscosity can also reduce the evaporation rate by suppressing the diffusion of molecules to the droplet surface. While there is a large body of research on characterizing the thermophysical properties of colloidal fluids, viscosity and surface tension variations seem to be strong functions of particle types, morphology and size. For example, Traciack and Zyla [21] explain that spherical nanoparticles will increase the surface tension while particle with a plate or tubular shape will decrease surface tension. Bhuiyan et al. [22] reported that the surface tension of nanofluids of Al_2O_3 and SiO_2 in distilled water increases with increase in particle concentration while Chinnam et al. [23] reported the opposite for nanofluid prepared by suspending Al_2O_3 and SiO_2 in a solution of propylene glycol and water. There is not much data available on physical properties of CFA suspensions or those of SWCNT in Jet-A fuel and as such it is crucial to measure them to better understand variations in evaporation and burning rate. To that end, an ATO digital rotational viscometer was used to measure viscosity, and a Kyowa DY-300 surface tensiometer, employing Wilhelmy plate method, was utilized to measure surface tension.

2.3. Evaporation rate, burning rate, and ignition delay measurements

To evaluate the burning/evaporation rate of nanofuels, a suspended droplet technique was employed. In this method, a small droplet of prepared sample is deployed on a 100-μm silicon carbide (SiC) fiber and is exposed to heat supplied by a custom-built heating element, as shown in Fig. 6. The fiber support holder, fabricated by 3D printing, consists of six vertical posts to hold a fiber, forming a place for droplet represented in Fig. 6-(A). Single droplets ranging from 0.7 mm to 1 mm in diameter were generated using a micro syringe (Hamilton 10 μL Syringe, Model 701). A 32-gauge Kanthal A-1 wire was used to build a heating element to evaporate or ignite the fuel droplets. The heating element wires passed through two alumina porcelain insulators and were connected to power source through a PCB terminal as illustrated in Fig. 6-(B). In Fig. 6-(C), the entire heating system is mounted on a solenoid and connected to a linear actuator, which is controlled via a pulse-width modulation (PWM) module. The main objective of this assembly is to provide a precise control over the distance between the heat source and droplet and also to retract the heat source in combustion experiments and preempt any potential interference with the flame. Finally, an Arduino Mega 2560 microcontroller board was employed to regulate the timing and sequence of the events. The evaporation/burning process was then captured by a high-speed camera (Photron SA4), at a rate of 500 fps for evaporation rate and 1000 fps for combustion experiments. The images are then analyzed by an image processing software, NASA Spotlight [24] to evaluate the droplet diameter and extract the droplet surface area regression rate as described by the d^2-law of evaporation/combustion through the following Equation:

$$\left(\frac{d(t)}{d_0}\right)^2 = 1 - K\left(\frac{t}{d_0^2}\right) \quad (1)$$

Where d, d_0, t, and K are droplet instantaneous diameter, droplet initial diameter, time, and evaporation/burning rate constant, respectively.

The addition of micro and nanoparticles can affect heat transfer within a liquid and its optical properties, hence affecting its ignition characteristics. The ignition delay in this study refers to the duration

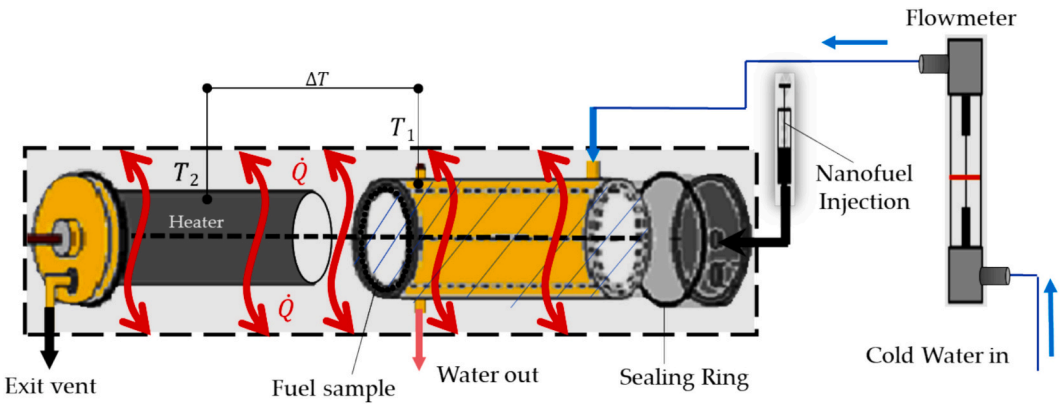

Fig. 5. Schematic of thermal conductivity measurement.

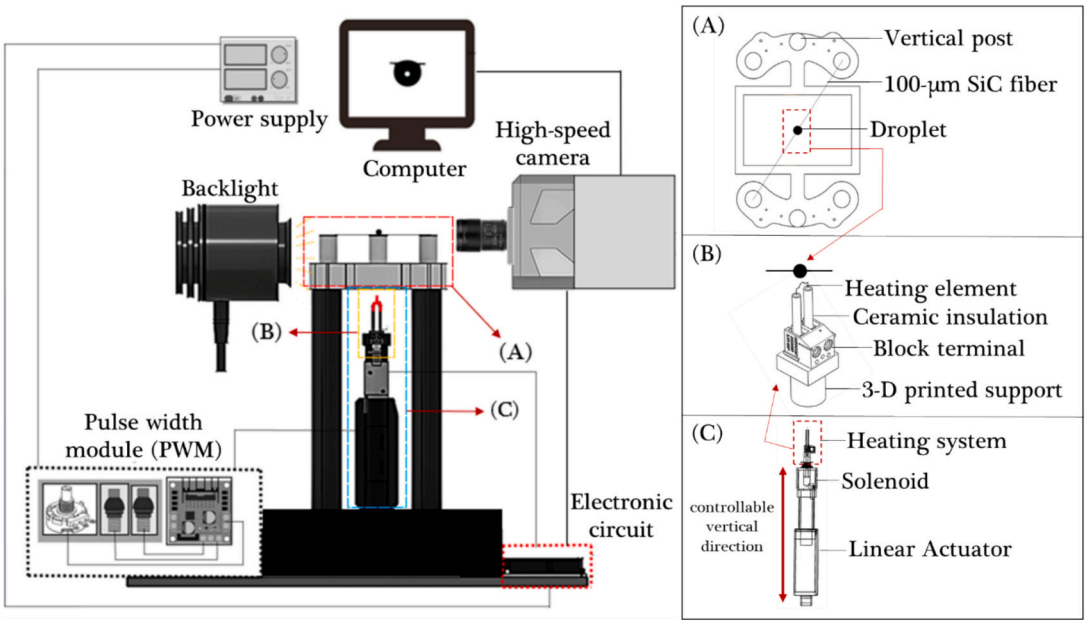

Fig. 6. Schematic of thermal evaporation/burning droplet combustion experimental apparatus; (A) Fiber support holder configuration, (B) Heating custom design, and (C) controlled system mobility.

required for ignition to start after the heating initiation. Both physical and chemical phenomena contribute to ignition delays. Physical delay arises from the time necessary for fuel vaporization and the formation of combustible blends, while chemical delay stems from the lag in fuel and air combustion reactions [25]. This study determined ignition delay through video recording and image sequence analysis. The ignition delay was quantified as the duration from the heating resistance activation frame to the flame's initial appearance in the video recording. Several measures were taken to reduce uncertainty across many trials, using the same length of the Kanthal wire to keep the same resistance and supplying the same voltage and current to guarantee equal heating power across all experiments. Finally, the linear actuator was used to carefully adjust a similar distance between the heating element and all droplets.

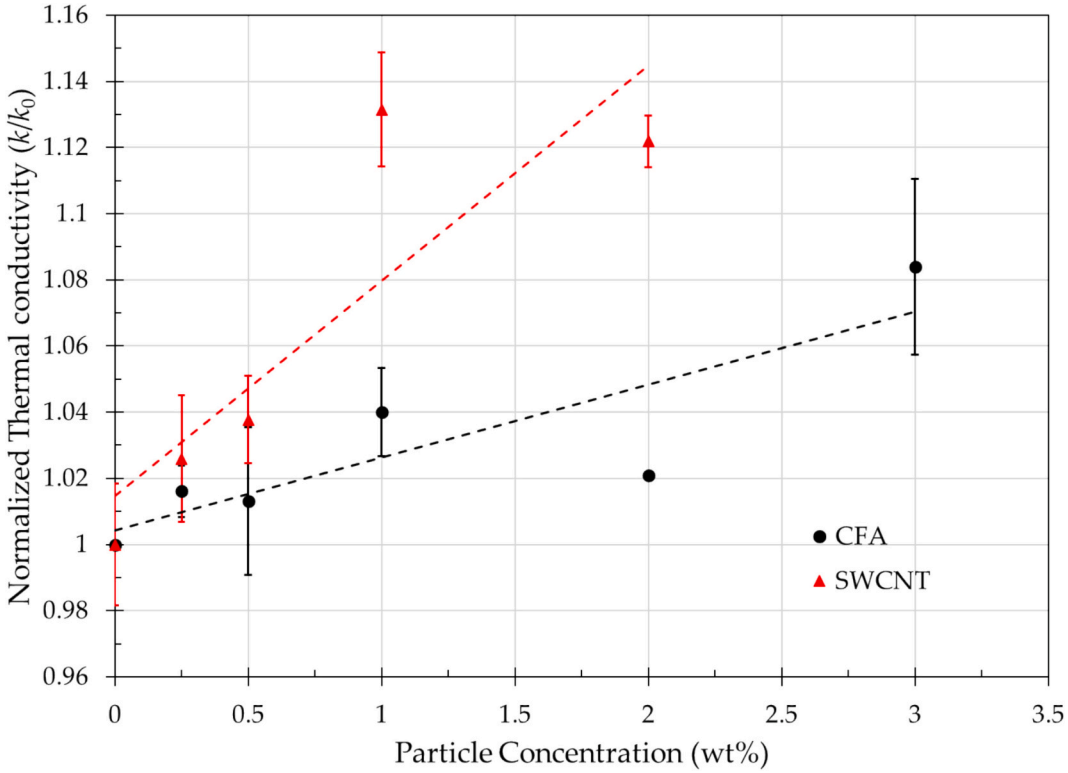

Fig. 7. Variation of normalized thermal conductivity of suspensions of CFA and SWCNT as a function of particle concentration and at a mean temperature of 36 °C (k_0 = 0.995 W/m·K; Error bars represent the standard deviation.)

3. Result and discussion

3.1. Thermal conductivity of suspended CFA and SWCNT in Jet-A fuel

The application of three distinct heat rates to each sample, coupled with temperature monitoring until achieving equilibrium, revealed marginal fluctuations in thermal conductivity at each particle concentration. The variation of the normalized thermal conductivity as a function of particle concentrations is displayed in Fig. 7. As evident by the trend shown in this Figure, adding both CFA and SWCNT results in a discernible enhancement in the thermal conductivity of the colloidal fuels. Several mechanisms, including nanoconvection due to Brownian

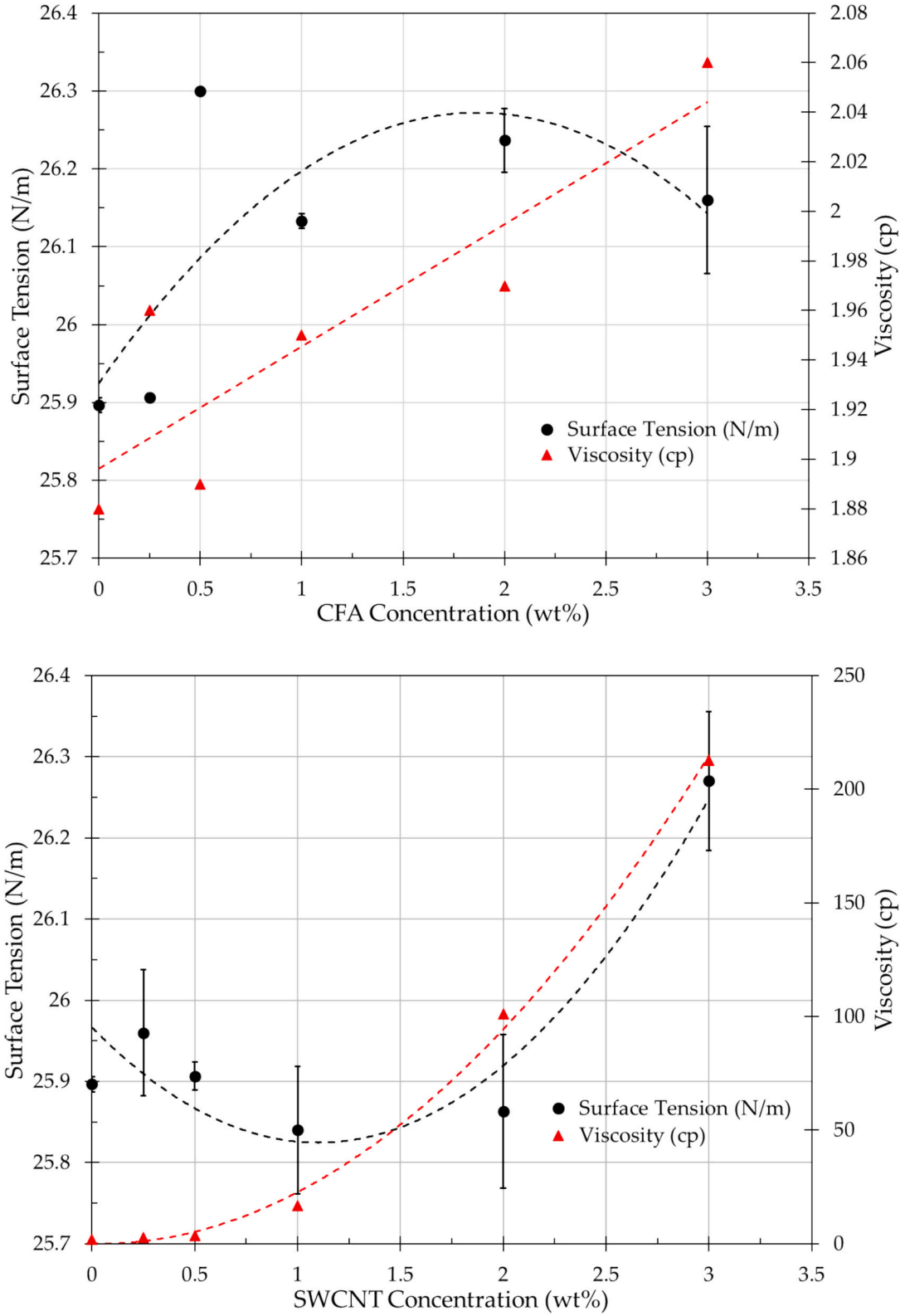

Fig. 8. Surface tension and kinematic viscosity of colloidal suspension of CFA and SWCNT in Jet-A fuel as a function of particle concentration.

motion of nanoparticles, thermal bridge between nanoparticles, and the formation of aggregates of nanoparticles, are believed to be responsible for such enhancement [15]. In the case of SWCNT, a remarkable 13 % enhancement in thermal conductivity was achieved at 1 wt%. This considerable increase can be attributed to the notably high thermal conductivity inherent to carbon nanotubes, rivalling that of natural diamond at 3000 W/m·K [26], or potentially surpassing it, being measured at an impressive 6600 W/m·K [27]. In contrast, only an 8 % increase was observed at the 3 % CFA concentration, which is on a par with the conductivity of 100 nm activated carbon nanoparticle in Jet-A fuel. It can also be in part attributed to the presence of trace amount of iron in CFA, as shown by Table 1. While an overall increase in thermal conductivity is observed upon CFA addition, a variability across a spectrum of heat conductivity rates is also visible. On the other hand, the distinctive porous morphology of the material, facilitating the uniform penetration of Jet-A fuel, reinforces the observed surge in thermal conductivity. Yet, disparities in particle sizes may precipitate swift agglomeration, posing a challenge to sustained enhancement of thermal conductivity. When comparing Carbon Fly Ash (CFA) with SWCNT, MWCNT, GNP, and CNP [15] in terms of thermal conductivity enhancement, CFA shows the smallest increase, largely due to its untreated nature and impurities. Specifically, an 8 % increase in thermal conductivity was observed at a 3 % CFA concentration, which is comparable to the conductivity of 100 nm CNP in Jet-A fuel. In the case of CNP, thermal conductivity begins to decrease at concentrations above 2 %. In contrast, SWCNT achieves a peak enhancement of 13.15 % at 2 wt %, significantly outperforming CFA. When compared to other carbon-based nanomaterials added to jet fuel [15], it is seen that MWCNT shows the most substantial improvement among all the materials, with a 29.37 % increase at 3.0 wt%. GNP demonstrates a moderate increase of 9.66 % at 2.0 wt%, only 1.66 % higher than CFA at its peak. CNP achieves a peak improvement of 12.77 % at 2.0 wt%, significantly better than CFA. This comparison clearly highlights that while CFA does exhibit some potential for enhancing thermal conductivity, MWCNT and SWCNT provide the most significant improvements, followed by CNP and GNP.

3.2. Viscosity and surface tension

In the analysis of CFA and SWCNT effects on the surface tension and viscosity of a suspension, distinct trends emerge, as shown in Fig. 8. While the viscosity of Jet-A fuel suspension increases almost linearly with the addition of CFA, the effect of SWCNT is visibly more pronounced and nonlinear. Bashirnezhad et al. [28] have reviewed models and theories predicting nanofluid viscosity μ_{nf} as a function of base fluid viscosity μ_{bf} and particles volume fraction φ. For example, the Einstein model (1906), shown by Eq. (2), can provide a prediction that has an excellent agreement with our experimental data for CFA suspensions, particularly at low mass fractions (less than 2.6 %, equivalent to volume fractions φ of less than 2 %).

$$\frac{\mu_{nf}}{\mu_{bf}} = [1 + 2.5\varphi] \tag{2}$$

However, the viscosity for SWCNT suspensions does not follow any of the established empirical or theoretical models, and the degree of nonlinearity is well beyond the models' predictions. Other studies have reported such a dramatic increase in the viscosity of SWCNT suspensions. For instance, Rudyak et al. [29] reported a 20-times increase in the viscosity of ethylene glycol, water, and isopropyl alcohol when doped with SWCNT at 0.05 % to 1 % concentrations. The measured viscosity of SWCNT suspensions in the current study shows a 16-fold increase at 1 % particle concentration that jumps to 101 times and 212 times increase at 1 % and 2 %, respectively.

The effect of particle addition on surface tension is similar for both CFA and SWCNT, resulting in a maximum increase of 1.5 %. However, the way surface tensions increase differs for CFA and SWCNT. CFA suspensions show a 1.5 % increase at a concentration as low as 0.5 % and maintain this level at higher concentrations. In contrast, SWCNT suspensions show little change up to 2 % concentration, but then begin to rise, reaching a 1.5 % increase at 3 % concentration. This difference in behavior can be attributed to the size difference between CFA and SWCNT. According to Tanvir and Qiao [30], for very small particle sizes or at very low concentrations, the distance between particles is still larger than the particle size, and not small enough to result in considerable attractive forces. However, for larger particle sizes or at higher concentrations, the Van der Waals force is large enough to lead to a higher free energy at the surface, and hence an increase in surface tension. This explains why larger CFA particles show an increase in surface tension at lower particle concentrations, while smaller SWCNTs require a higher concentration to observe any change in surface tension.

3.3. Evaporation of suspended isolated droplets

The evaporation process of fuel droplets including CFA and SWCNT was observed to undergo three distinct stages, as shown in Fig. 9: initial particle interaction with the base fuel accompanied by droplet swelling due to thermal expansion followed by smooth and stable evaporation and culminating in evaporation of an unstable suspension. During the initial Stage, particle interaction was facilitated by impinging interaction and Brownian motion, resulting in a normalized diameter of $(d/d_0)^2 > 1$. In the second Stage, the interaction of particles with the base fuel was intensified by the enhanced conductivity and convective effects, leading to increased particle movement and establishing a stable suspension. The normalized diameter range during this Stage was typically in the range of $0.4 < (d/d_0)^2 < 1$, resulting in a higher evaporation rate compared to the base fuel. This range encapsulates the data points used to evaluate the constant evaporation coefficient, due its linear slope with negligible curvature. Performing a visual comparison between the images of both SWCNT and CFA droplets, it was revealed the agglomeration of fly ash particles occurred at a faster rate, likely due to their size being several orders of magnitude larger than that of nanotubes. This led to a more rapid escape of fuel to the interface and the formation of particle clusters that obstructed the evaporation process.

The third Stage was characterized by an unstable suspension within the interval $(d/d_0)^2 < 0.4$. The agglomeration of particles in this phase was instrumental in suppressing molecular diffusion to the surface and reducing fuel evaporation. It was also observed that the flame extinction occurs at a relatively larger diameter for SWCNT colloidal droplets compared to CFA ones. The porous structure of CFA particles may have contributed to this phenomenon, indicating that nearly all the fuel was evaporated with the aid of these particles. Fig. 10 (i) presents a detailed depiction of the evaporation dynamics of a CFA colloidal droplet, initially measuring 0.77 mm in diameter, showcasing a stable suspension. The droplet maintains a spherical shape on the fibers, following a linear regression of the evaporation rate that reduces its diameter to 0.51 mm by $t = 5.2$ s. By $t = 7.1$ s, signs of agglomeration emerge, although complete coalescence has not yet occurred. The base fuel remains able to interact with the gas phase, resulting in a noticeable decrease in droplet diameter to 0.41 mm. In contrast, Fig. 10 (ii) portrays the evaporation progression of a 0.5 % SWCNT colloidal droplet, initially 0.8 mm in diameter. The Figure exhibits a stable suspension of the droplet, albeit with an irregular distribution of SWCNT, maintaining a spherical shape. Following a linear regression of the evaporation rate, the droplet diameter decreases to 0.57 mm by $t = 6.5$ s, showing a slower rate compared to that of CFA. As time advances to $t = 9.6$ s, agglomeration commences, culminating in complete particle coalescence. Here, the base fuel loses its ability to interact effectively with the gas phase, leading to a significant reduction in evaporation rate.

Fig. 11 presents the evaporation rate k, in mm^2/s, of CFA and SWCNT in Jet-A fuel, revealing notable performance disparities. At a CFA concentration of 0.25 %, there is a substantial 29 % increase compared to

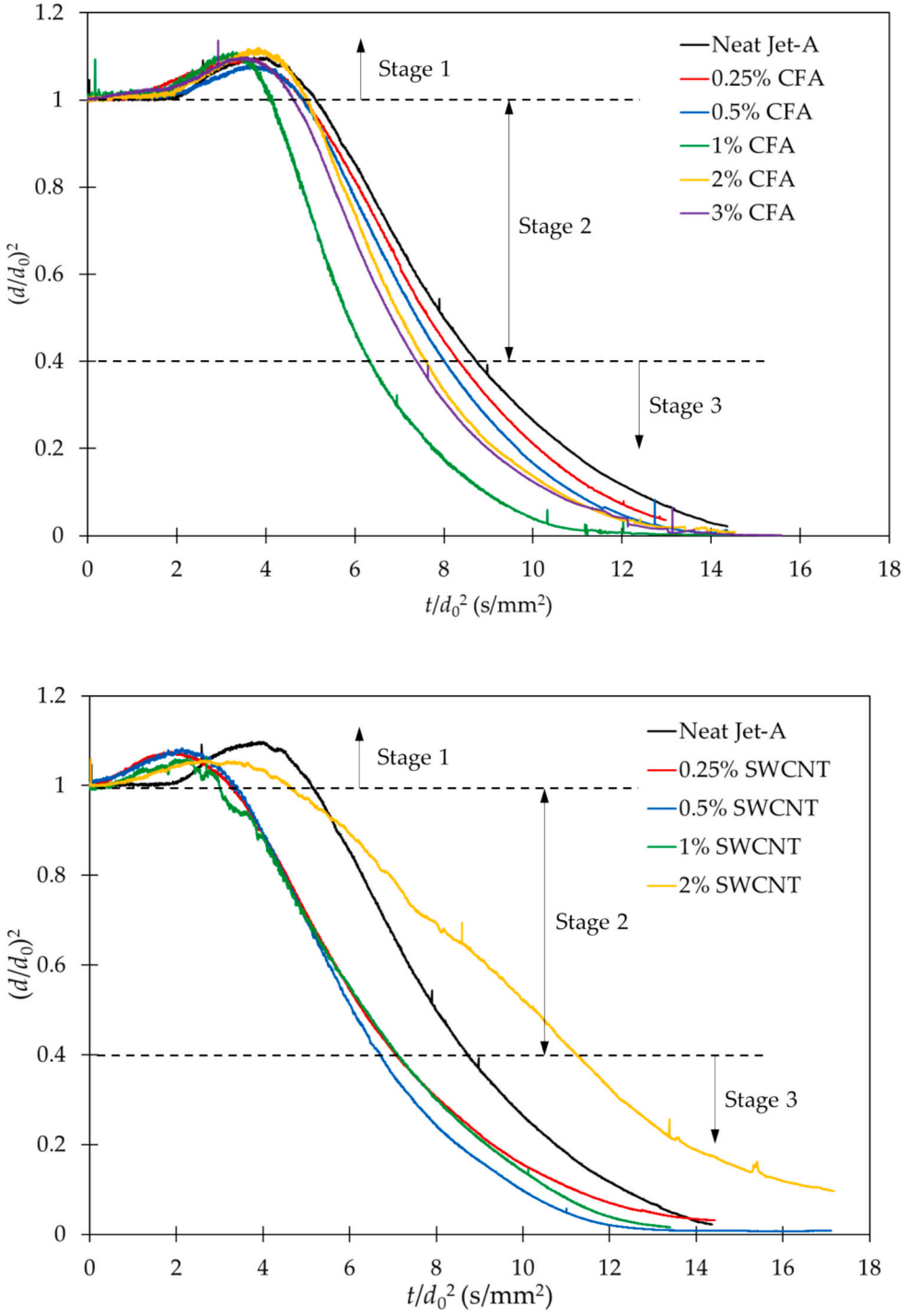

Fig. 9. Evolution of normalized diameter square for colloidal suspensions of CFA and SWCNT in Jet-A fuel.

20 % at the same SWCNT concentration, while at 0.5 % concentration CFA suspensions demonstrate a remarkable 32 % rise compared to the base fuel. This prompts an inquiry into whether this escalation will impact the burning rate during combustion. Interestingly, at 1 % concentration, CFA exhibits 87 % increase, whereas SWCNT suspensions show a contrasting decrease compared to CFA, albeit with a modest 7 % increase over neat Jet-A fuel. Notably, CFA concentrations of 2 % and 3 % display significant increases of 75 % and 69 %, respectively, whereas SWCNT experience a drastic 36 % decrease at 2 % particle loading, as evident in the linear regression depicted in Fig. 9. Particularly at 2 % SWCNT, unstable evaporation and a distinctly smaller linear regression slope are observed, setting it apart from other concentrations.

3.4. Combustion of suspended isolated droplets

The study's findings underscore that the combustion burning rate exhibited a relatively higher magnitude in comparison to conventional Jet-A fuel. Remarkably, all concentrations exhibited analogous stages in their combustion trajectories, as shown in Fig. 12. Stage (a) is initiated by activating the heating element that prompts heating expansion at a rate faster than evaporation, leading to a discernible swelling. Subsequent to this, the ignition process ensues, as illustrated by Figs. 13–2, giving rise to a visible flame. Notably, a sooty flame becomes apparent, effectively absorbing radiation emitted from the ignited droplet. This soot layer functions as a supplementary heat energy carrier, augmenting

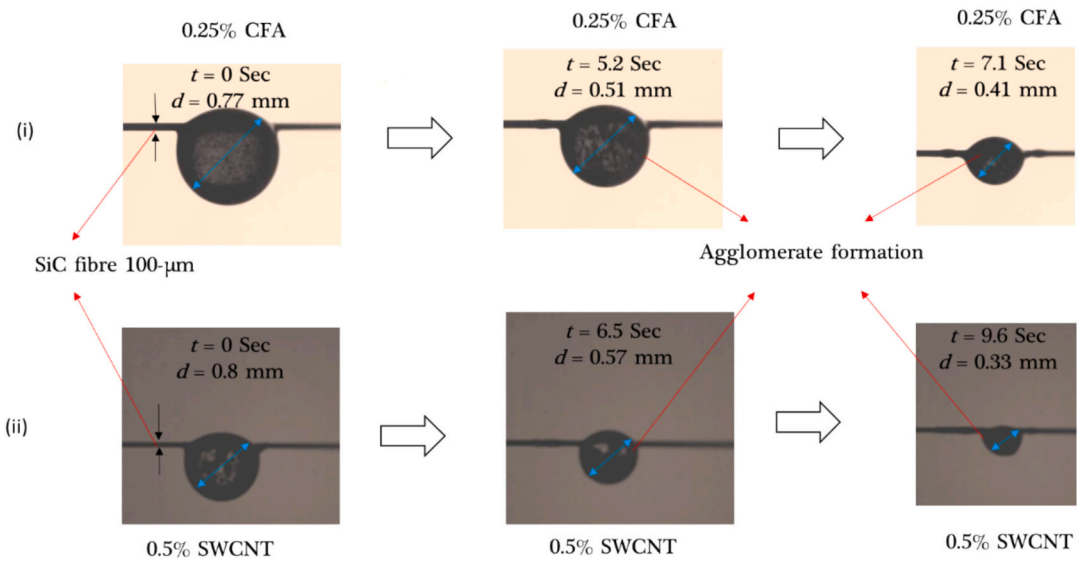

Fig. 10. Time lapse of agglomerate formation in a droplet of (i) 0.25 % CFA and (ii) 0.5 % SWCNT in Jet-A fuel.

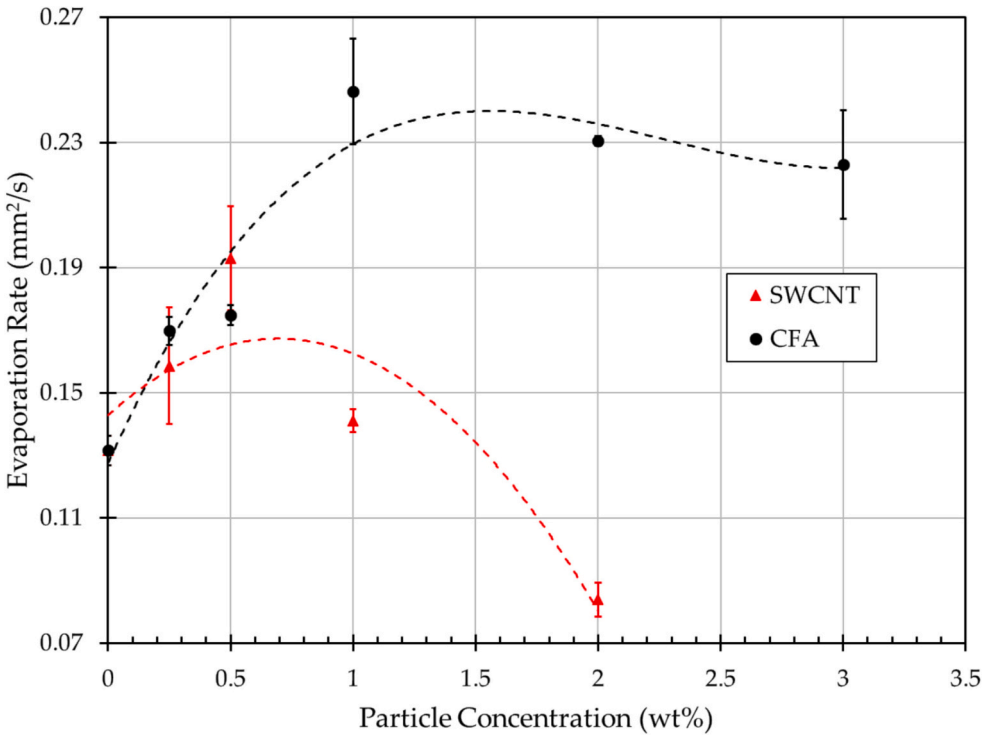

Fig. 11. Variation of droplet burning rate (K_{evap}) for colloidal suspensions of CFA and SWCNT in Jet-A fuel.

combustion temperature and thus accelerating the combustion process. The droplet then transitions into the smooth combustion Stage (b), during which a relatively less pronounced swellings and puffings occur. Subsequently, the droplet enters the Stage where its internal constituents begin to coalesce as the presence of more particles per unit volume renders higher probability of collision. The paramount event at this Stage is the mass loss due to puffing, also known as secondary atomization, that results in the formation of smaller spherical droplets or ligaments that eject from the immobilized droplet surface to the liquid evaporation phase zone, and from there to the flame zone. Observations through a magnifying lens indicate that the droplet undergoes several stages of internal boiling and bubble formation due to different boiling points of surfactant and base fuel, and presence of particles as nucleation sites.

The internal pressure dynamics within the droplet are also influenced by the added surfactant, as depicted in Fig. 13–4. As the more volatile base fuel evaporates and burns, the surfactant, as one of the less volatile components, experiences rise in concentration. The regions near the droplet surface are exposed to more intensive radiation and as such the surfactant will start to decompose and degrade, hence forming volatiles that lead to bubble growth and subsequent moderate-intensity puffing. Fig. 13–5 captures the deformation of the droplet, culminating in a pronounced micro-explosion. These phenomena unfold in the preliminary stages preceding Stage (b) and reach completion during Stage (c), as shown in Fig. 12. In this Case, CFA agglomerate assumes the role of a small, micron-scale envelope, selectively attracting carbon-rich

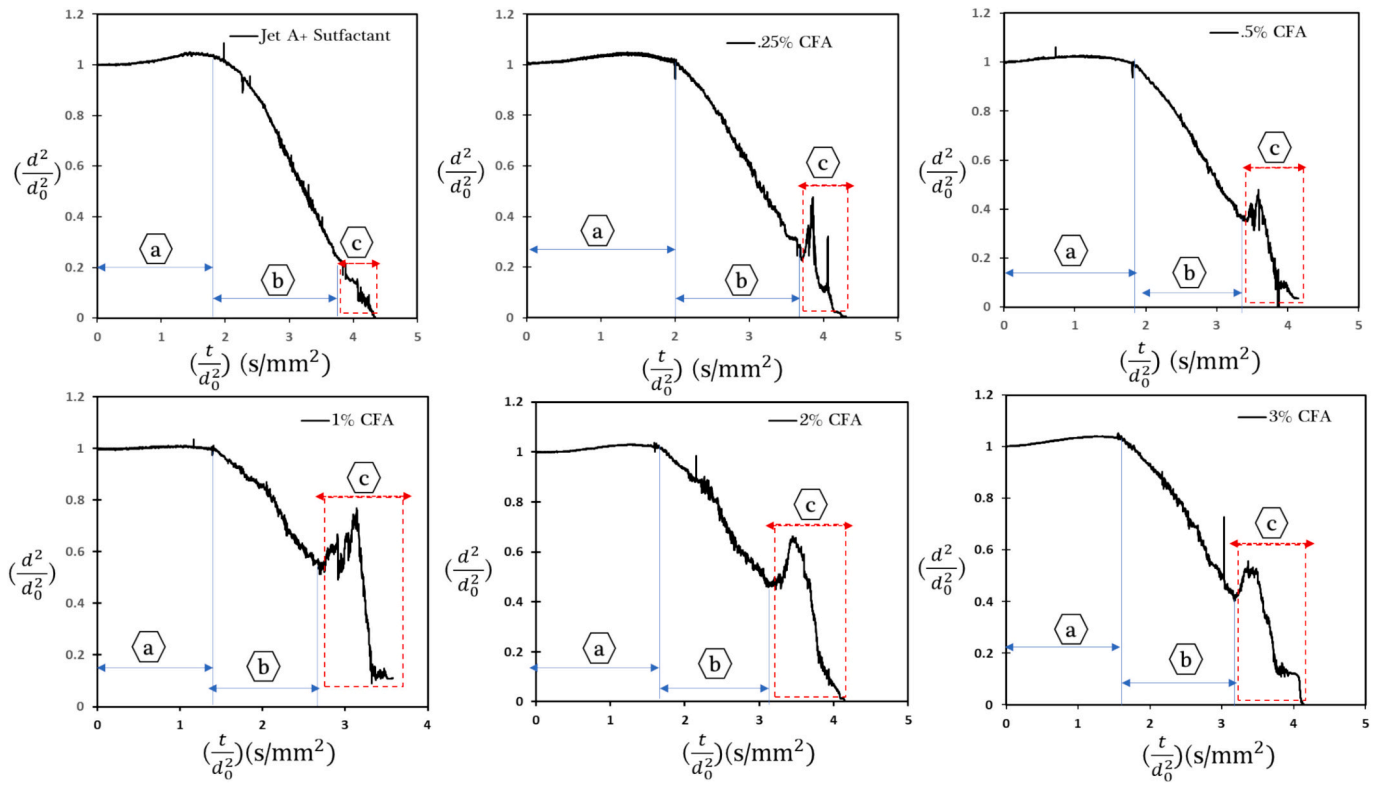

Fig. 12. Evolution of normalized droplet diameter square for colloidal suspensions of CFA in Jet-A fuel at different concentrations.

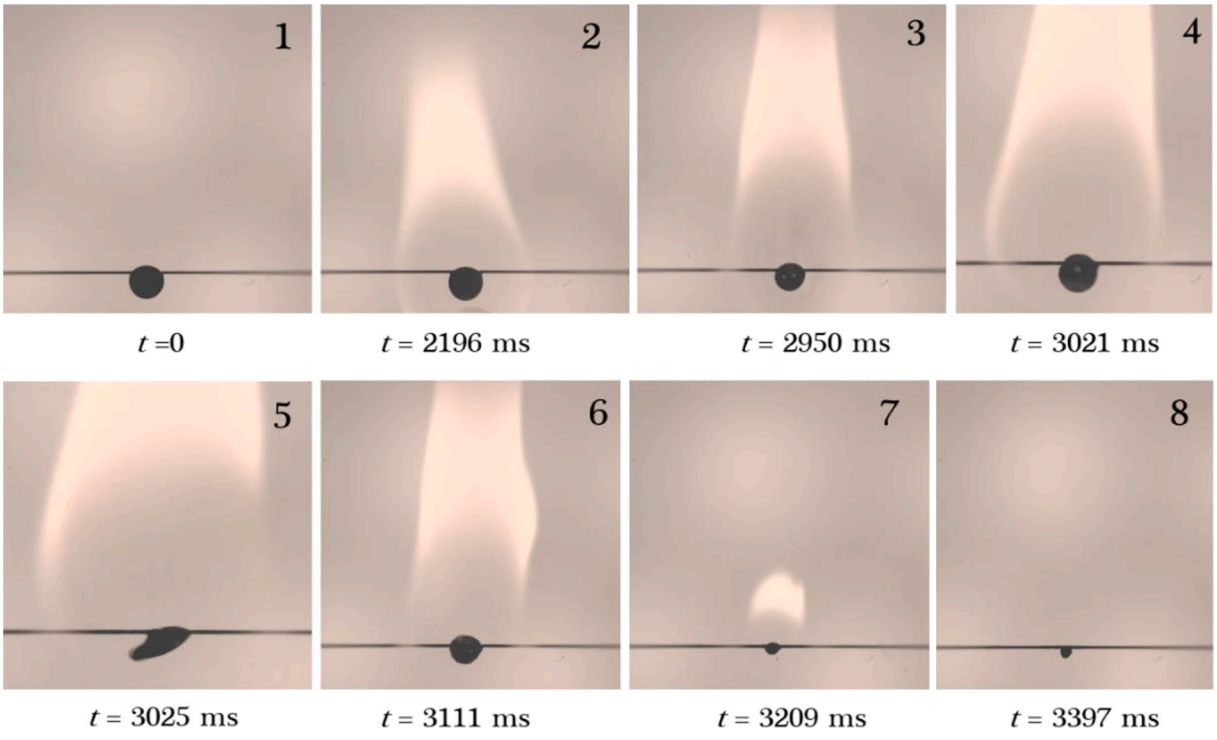

Fig. 13. Droplet combustion dynamic of the Jet A fuel+1 % CFA.

particulates. The porous structure of CFA agglomerate allows the penetration of the base fuel, which, due to differences in boiling points between the surfactant and the base fuel, constantly expels foamy bubbles, as shown in Fig. 13–6. Gradually, this foamy structure inflates, and the early signs of micro-explosions become evident. This phenomenon is depicted in Fig. 12, Stage (c), where the presence of a peak, followed by a rapid decline within a few moments, signifies the vigor of this occurrence near the end of combustion.

In the ultimate Stage of droplet combustion, the flame gradually fades away, only to reappear suddenly with a higher intensity just before

extinction. Notably, after the flame vanishes, the residual carbonaceous materials remain, emitting a radiant glow. The observed phenomenon can be attributed to the substantial proportion of carbon that has not yet undergone complete combustion, retaining stored energy. Additionally, the combustion of the surfactant, initially trapped within the micro-sized carbonaceous particle pores, contributes to this incandescence. It is worth mentioning that in the absence of any surfactant, there is a complete separation of base fuel and particles, leading to a steady combustion with the particles agglomerated at the center and not going through combustion. However, adding surfactant delays agglomeration and helps particles to suspend longer, leading to nucleation, boiling, and the secondary atomization.

A similar experimental methodology was employed to study the combustion of SWCNT in Jet-A fuel. The initial Stage (a), shown in Fig. 14, entails preheating, expansion, and ignition, succeeded by a secondary Stage (b) marked by steady combustion with minor fluctuations, adhering to the classical d^2-law of droplet combustion. In comparison with CFA cases, the combustion in this Stage manifests reduced violent puffing and minimal ejection of droplets, while suspensions of CFA exhibit more intense puffing accompanied by the pronounced ejection of daughter droplets. As Stage (c) unfolds, agglomeration accelerates, precipitating the deposition of agglomerated particles onto the SiC fiber. Combustion stages for droplet containing 0.5 % SWCNT is shown in Fig. 15.

Fig. 16 shows the average normalized diameter square at which droplet combustion transition from Stage (b) to Stage (c). It is clear that CFA suspension transition to bubbling and microexplosion at a much smaller droplet size. Considering microexplosion being caused by nucleation around the particles near the surface, Fig. 16 suggests that CFA particles escape toward the droplet center at faster rate at higher particle loadings. SWCNT suspension, on the other hand, show little to no sensitivity to particle loading when it comes to transition from steady to unsteady combustion. SWCNT are in general more susceptible to entangle around each other and form agglomerate. As such, while CFA tendency to coalesce increases with their count in droplet, SWCNT begin to agglomerate at a faster rate and lower concentrations.

The droplet burning rate defined as the speed of droplet surface regression can be estimated using the slope of a line passed through the data points ($0.2 < (d/d_0)^2 < 1$) representing combustion in Figs. 12 and 14. The average burning rate constant (k, in mm^2/s) for each particle concentration is shown in Fig. 17 with the error bars representing the standard deviation. These data show a notable increase in burning rate when compared to neat Jet-A fuel. For CFA suspension, Fig. 17 demonstrates that at 0.25 % and 0.5 % concentrations the burning rate increases by a modest 2 %. However, the burning rate increases as more particles are added until a remarkable 9 % increase was recorded at a particle concentration of 1 %. Subsequent concentrations of 2 % and 3 % resulted in burning rate reduction, but yet 5 % higher than that of neat fuel. In contrast, the performance of the droplet burning rate constant with the addition of SWCNT shows a pronounced increase compared to CFA. As shown in Fig. 17, a significant enhancement of 15 % was observed at 0.25 % SWCNT concentration. The increase in burning rate peaked at a sharp 25 % for 0.5 % concentration. The burning rate dropped at higher concentrations showing only 11 % and 8 % increase for 1 % and 2 % particle concentrations, respectively. The drop in burning rate after its initial increase can be attributed to the possible

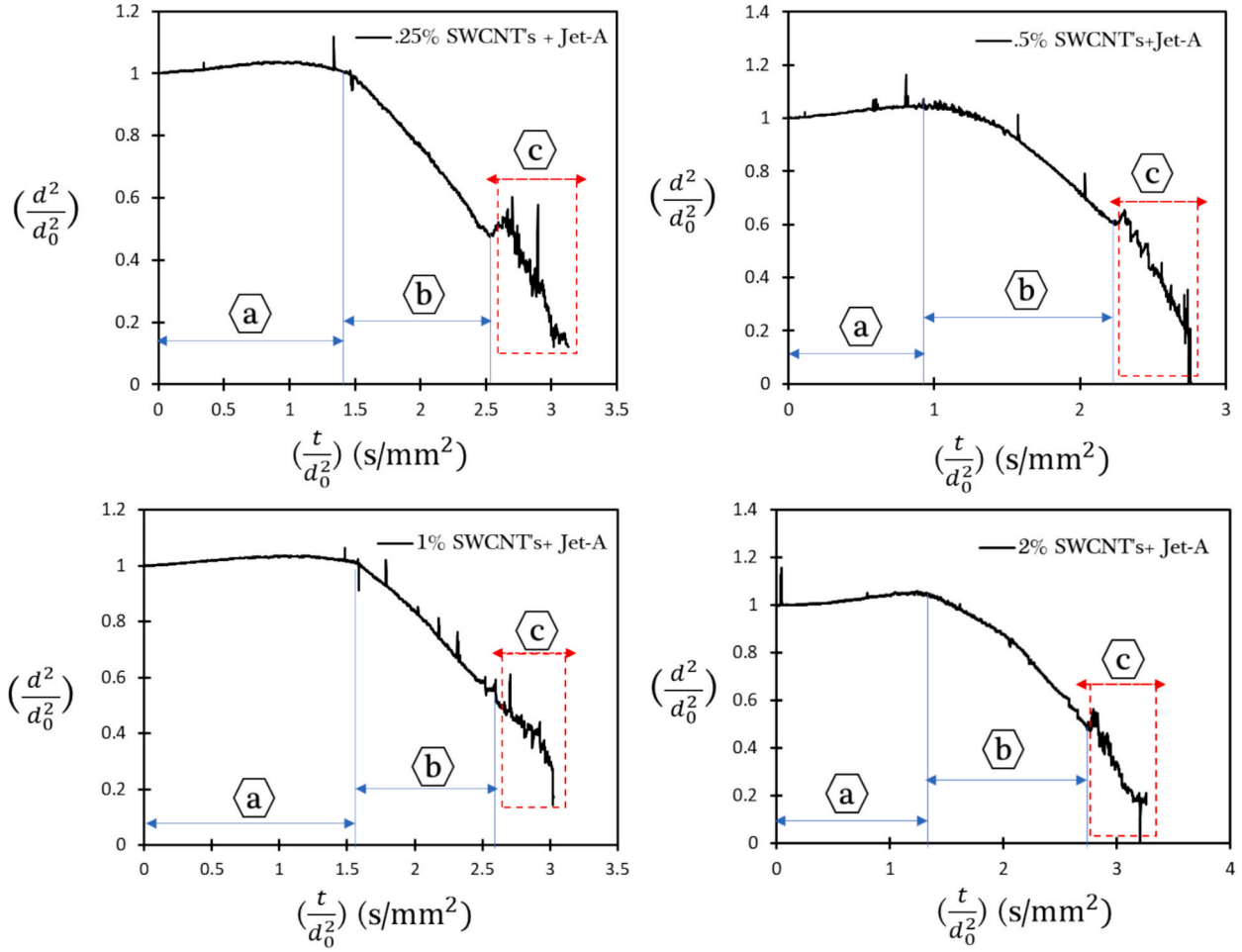

Fig. 14. Evolution of normalized droplet diameter square for colloidal suspensions of SWCNT in Jet-A fuel at different concentrations.

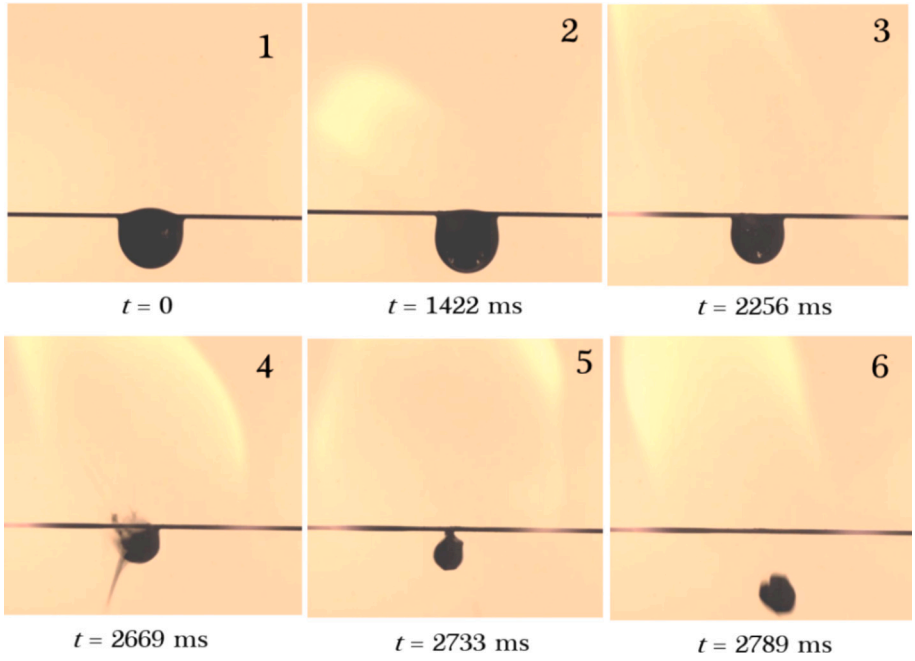

Fig. 15. Droplet combustion dynamic of the Jet-A fuel+0.5 % SWCNT.

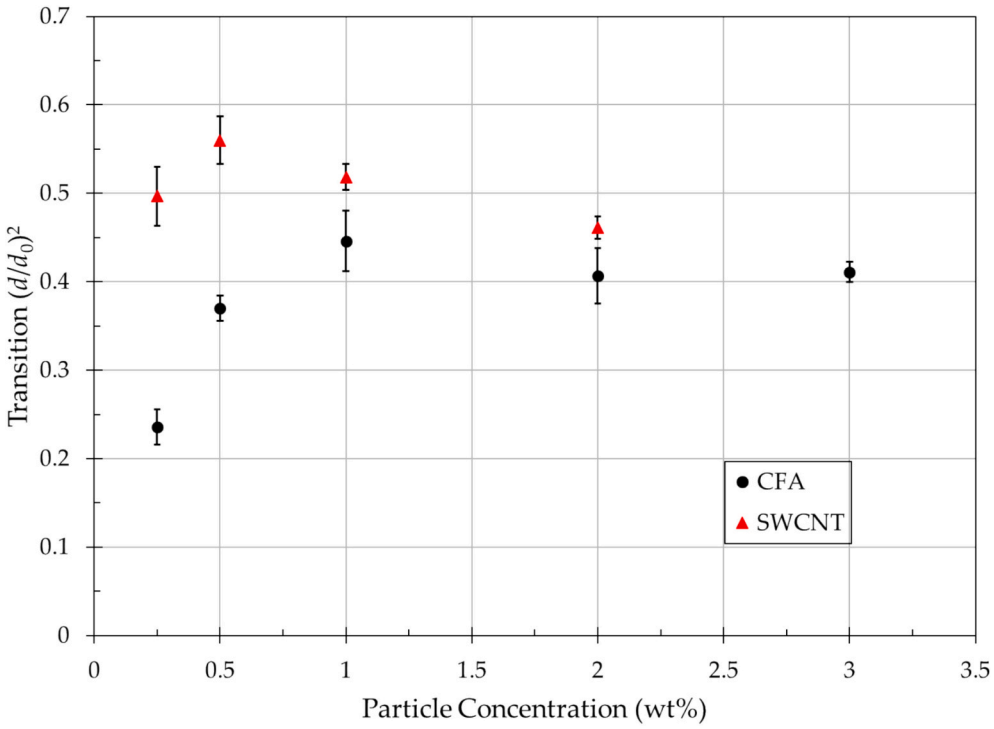

Fig. 16. Variation of normalized diameter for transition from Stage (b) to Stage (c), as shown in Figs. 12 and 14.

agglomeration of particle as well as increase in the local particle concentration that may suppress the diffusion of liquid fuel toward the droplet surface. While higher thermal conductivity at higher particle concentrations may enhance heat distribution within the droplet, heightened viscosity can lead to a higher shear rate and suppress internal circulation and molecular diffusion. Increased surface tension can inversely affect evaporation too but the small 1.5 % increase in surface tension may be insignificant to cause any meaningful change.

3.5. Ignition delay

Fig. 18 illustrates the ignition delay of suspensions containing CFA and SWCNT in Jet-A fuel, accompanied by error bars. Notably, the results indicate a significant reduction in ignition delay for CFA at a concentration of 0.5 % compared to the base fuel. Conversely, SWCNT at a concentration of 0.5 % exhibits the most favorable ignition delay enhancement relative to other particle mass concentrations. The ignition delay primarily depends on the rate at which the droplet absorbs heat (thermal conductivity) and releases vapor (vapor pressure). Lower

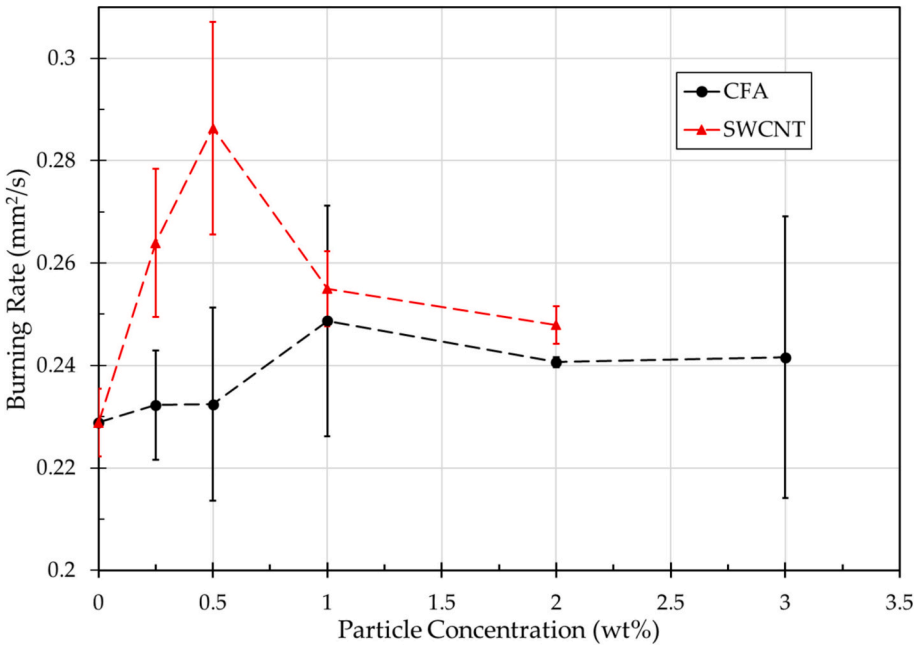

Fig. 17. Variation of droplet burning rate (K_{burn}) for colloidal suspensions of CFA and SWCNT in Jet-A fuel.

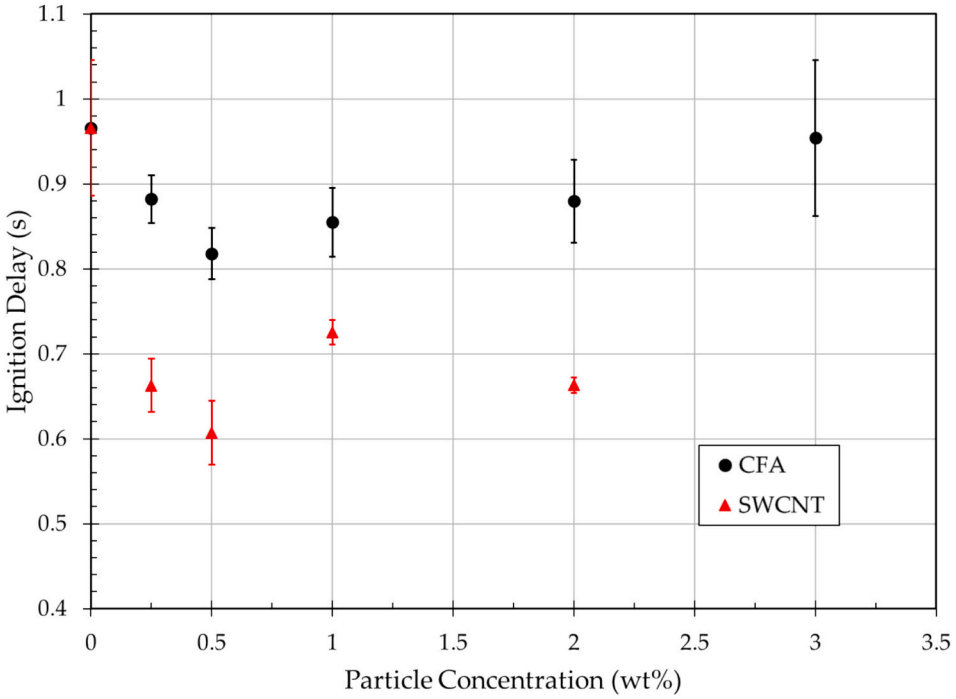

Fig. 18. Variation of ignition delay for colloidal droplets of CFA and SWCNT in Jet-A fuel.

thermal conductivity leads to a longer ignition delay, while lower vapor pressure also results in an increased ignition delay [31,32]. Additionally, the inherent high conductivity of SWCNT further facilitates rapid ignition. Ninety-five percent of the material supplied were CNTs, and of these, 90 % were SWCNT. SWCNT is Manufacturing method Catalytic CVD which involves Cobalt (Co), like iron (Fe), is commonly used as a catalyst for carbon nanotube synthesis. Both metals help in the decomposition of carbon-containing gases during the CVD process, facilitating the growth of SWCNT [33]. In particular, cobalt is known for producing high-quality nanotubes with specific diameters and structures due to its catalytic properties. In different studies the amount of iron varies as in instance in this study iron content in SWCNT is 0.23 % to study Induction of Aneuploidy [34]. The iron (Fe) nanoparticles in the SWCNT vary in size and morphology it is more spherical as the study by Guo, L et al. [35]. The pristine SWCNT initially contain iron nanoparticles with diameters ranging from 1 to 5 nm [36]. These nanoparticles are distributed both within the nanotube bundles and along their exterior surfaces. After ignition, the iron nanoparticles tend to coalesce, leading to a significant increase in size, sometimes exceeding 100 nm in diameter due to melting during the combustion process. These iron nanoparticles, embedded within the SWCNT, play a crucial role in the ignition process of fuels by facilitating localized heat generation when exposed to a

stimulus such as heat (radiation) heating system in this research, leading to fuel ignition. The interaction of iron nanoparticles with oxygen during this process results in the formation of iron oxides (Fe_2O_3 and Fe_3O_4) [37], which further contributes to the heat release during combustion [38,39]. The iron nanoparticles, due to their catalytic properties and size, enhance the reactivity and heat generation needed for efficient fuel ignition, thereby affecting combustion characteristics like ignition delay and burn rate.

4. Conclusion

This study systematically investigated the thermophysical properties of colloidal suspensions of carbon-rich fly ash (CFA) microparticles and single-walled carbon nanotubes (SWCNT) in Jet-A fuel, focusing on their impact on evaporation rates, burning rates, and ignition delays. The experimental findings are summarized as follows:

- The addition of SWCNT to Jet-A fuel resulted in a remarkable enhancement in thermal conductivity, with a 13 % increase observed at a 1 % concentration. In contrast, CFA showed a more modest improvement, with an 8 % increase at a 3 % concentration. The higher thermal conductivity observed with SWCNT is attributed to their superior intrinsic thermal properties (measured at 6600 W/m·K) and the catalytic presence of iron nanoparticles on their surface.
- The viscosity of the Jet-A fuel suspensions showed a significant non-linear increase with SWCNT, where a 1 % concentration led to a 16-fold increase, escalating to a 212-fold increase at a 2 % concentration. CFA, on the other hand, caused a more linear increase in viscosity, with a maximum increase of 3.2 times at a 3 % concentration. This drastic rise in viscosity with SWCNT is indicative of their strong intermolecular interactions and potential agglomeration, especially at higher concentrations.
- The surface tension of the fuel suspensions increased by a maximum of 1.5 % for both CFA and SWCNT, albeit with differing trends. CFA caused this increase at a low concentration of 0.5 %, maintaining it at higher concentrations. In contrast, SWCNT required a 3 % concentration to achieve the same level of increase, likely due to their smaller size and the greater distance between particles at lower concentrations, which reduced van der Waals forces.
- The evaporation rate showed a substantial enhancement with the addition of CFA, reaching an 87 % increase at a 1 % concentration, which is significantly higher than the 7 % increase observed with SWCNT at the same concentration. This performance disparity is attributed to the larger size and porous morphology of CFA particles, which facilitated better interaction with the fuel and faster evaporation. CFA also showed a 75 % increase at a 2 % concentration and 69 % at a 3 % concentration, whereas SWCNT experienced a 36 % decrease at 2 % concentration, indicating instability and agglomeration issues at higher loadings.
- The combustion rate of the fuel was markedly improved with the addition of SWCNT, with a peak increase of 25 % at 0.5 % concentration, followed by 11 % and 8 % increases at 1 % and 2 % concentrations, respectively. CFA, on the other hand, showed a more gradual improvement, with a 9 % increase at 1 % concentration. Higher concentrations of CFA (2 % and 3 %) resulted in a slight decrease in combustion rate, but still remained 5 % higher than neat Jet-A fuel. The reduction in combustion rate at higher concentrations is likely due to the increased viscosity and agglomeration of particles, which impeded the diffusion of fuel molecules.
- SWCNT significantly reduced the ignition delay of Jet-A fuel, with the most pronounced effect observed at 0.5 % concentration, which showed a 24 % reduction compared to the base fuel. CFA also contributed to a reduction in ignition delay, particularly at a 0.5 % concentration, but the effect was less pronounced compared to SWCNT. The superior performance of SWCNT in reducing ignition delay is attributed to their high thermal conductivity and the presence of catalytic iron nanoparticles, which facilitated faster heat transfer and ignition.

Ethics and compliance

The authors declare that the study complies with ethical standards and, where applicable, necessary permissions have been obtained for the work conducted.

CRediT authorship contribution statement

Ahmed Aboalhamayie: Writing – original draft, Visualization, Validation, Methodology, Investigation, Formal analysis, Data curation, Conceptualization. **Nadeem Ahmad:** Methodology, Investigation, Data curation. **Yang Zhang:** Supervision, Resources, Project administration. **Mohsen Ghamari:** Writing – review & editing, Validation, Supervision, Formal analysis. **Numan Salah:** Writing – review & editing, Resources. **Jameel Alshahrani:** Methodology, Investigation.

Declaration of competing interest

The authors declare that they have no known competing financial interests or personal relationships that could have appeared to influence the work reported in this paper.

Acknowledgements

This work has been supported by the Saudi Arabia Cultural Bureau in London in a PhD scholarship to AA. One of the authors (Numan Salah) is thankful for the Research, Development, and Innovation “Authority (RDIA) - Kingdom of Saudi Arabia – for providing the grant number (12965-kau-2023-KAU-R-3-1-SE-).

Data availability

Data will be made available on request.

References

[1] C.W. Turner, D. Steve, Energy Management Handbook, 7th ed., The Fairmont Press, Inc, Lilburn, Georgia, 2009.
[2] S.L. Tsai, M.S. Tsai, Study on the physical and chemical characteristics, yield and TCLP test of oil-fired fly ash, Min. Metal 41 (2) (1997) 57–68.
[3] Y.M. Hsieh, M.S. Tsai, Physical and chemical analyses of unburned carbon from oil-fired fly ash, Carbon 41 (2003) 2317–2324.
[4] W.T. Kwon, D.H. Kim, Y.P. Kim, Characterization of heavy oil fly ash generated from a power plant, Azo J. Mater. Online (2005), https://doi.org/10.2240/azojomo0135.
[5] N. Salah, S. Habib, Z. Khan, A. Alshahrie, A. Memic, A. Al-Ghamdi, Carbon rich fly ash and their nanostructures, Carbon Lett. 19 (2016) 23–31.
[6] Y.H.M. Amran, M. Gutierrez Soto, R. Alyousef, M. El-Zeadani, H. Alabduljabbar, V. Aune, Performance investigation of high-proportion Saudi-fly-ash-based concrete, Results Eng. 6 (2020) 100118.
[7] A. Algarni, N. Salah, M. Bourchak, A. Jilani, A. Alshahrie, M.N. Nahas, Polymer composite reinforced with nanoparticles produced from graphitic carbon-rich fly ash, J. Compos. Mater. 51 (18) (2017) 2675–2685.
[8] A. Saeed, A. Alaqab, E. Banoqitah, M.M. Damoom, N. Salah, Graphitic carbon rich oil fly ash as effective reinforcements to enhance the mechanical, thermal, and radiation shielding properties of high-grade epoxy polymer, Polym. Test. 115 (2022) 107739.
[9] S.I. Basha, A.M. Kumar, M. Maslehuddin, S. Ahmad, M.M. Rahman, M. Shameem, A.S. Hakeem, M.A. Aziz, Preparation of submicron−/nano-carbon from heavy fuel oil ash and its corrosion resistance performance as composite epoxy coating, J. Clean. Prod. 319 (2021) 128735.
[10] N. Salah, A. Alshahrie, N.D. Alharbi, M.S. Abdel-wahab, Z.H. Khan, Nano and micro structures produced from carbon rich fly ash as effective lubricant additives for 150SN base oil, J. Mater. Res. Technol. 8 (1) (2019) 250–258.
[11] J. Yin, W. Zhang, G. Huang, N.A. Alhebshi, N. Salah, M.N. Hedhili, H.N. Alshareef, Fly ash carbon anodes for alkali metal-ion batteries, ACS Appl. Mater. Interfaces 13 (22) (2021) 26421–26430.
[12] Salah N, Abdel-wahab MS, Memic A, Alshahrie A, Aslam M. Method for removing polycyclic aromatic hydrocarbons from water using ball milled and sonicated oil fly ash powder. U.S. Patent No. 10,882,022 B2, 2021.

[13] A.K. Singh, Thermal conductivity of nanofluids, Def. Sci. J. 58 (5) (2008) 600.
[14] M. Ghamari, A. Ratner, Combustion characteristics of colloidal droplets of jet fuel and carbon based nanoparticles, Fuel 188 (2017) 182–189.
[15] A. Aboalhamayie, L. Festa, M. Ghamari, Evaporation rate of colloidal droplets of jet fuel and carbon-based nanoparticles: effect of thermal conductivity, Nanomaterials 9 (9) (2019) 1297.
[16] M.J. Ziabakhsh Ganji, H. Ghassemi, Evaluation of the solid particle from heavy fuel oil and its formation trend, Powder Technol. 427 (2023) 118744.
[17] T.A. Bui, N.T. Bui, Investigating the impact of fly-ash additive on viscosity reduction at different temperatures: a comparative analysis, Appl. Sci. 13 (2023) 7859.
[18] S.M. Chaudhari, S.V. Thakare, K.G. Sontakke, R.R. Khodke, Effect of metal based additives on a CI engine fuelled with diesel and water, J. Emerg. Technol. Innov. Res. 1 (7) (2014) 783.
[19] M. Fujii, X. Zhang, H. Xie, H. Ago, K. Takahashi, T. Ikuta, H. Abe, T. Shimizu, Measuring the thermal conductivity of a single carbon nanotube, Phys. Rev. Lett. 95 (6) (2005) 065502.
[20] H. Tyagi, P.E. Phelan, R. Prasher, R. Peck, T. Lee, J.R. Pacheco, P. Arentzen, Increased hot-plate ignition probability for nanoparticle-laden diesel fuel, Nano Lett. 8 (2008) 1410–1416.
[21] J. Traciak, Z. Gawel, Effect of nanoparticles saturation on the surface tension of nanofluids, J. Mol. Liq. 363 (2022) 119937.
[22] M.H.U. Bhuiyan, R. Saidur, M.A. Amalina, R.M. Mostafizur, A.K.M.S. Islam, Effect of nanoparticles concentration and their sizes on surface tension of nanofluids, Procedia Eng. 105 (2015) 431–437.
[23] J. Chinnam, D.K. Das, R.S. Vajjha, J.R. Satti, Measurements of the surface tension of nanofluids and development of a new correlation, Int. J. Therm. Sci. 98 (2015) 68–80.
[24] R. Klimek, T. Wright, Spotlight: Image Analysis and Object Tracking Software [Online], Available online, https://ntrs.nasa.gov/search.jsp?R=20060011194, 2004.
[25] A. Gallego, K. Cacua, D. Gamboa, J. Rentería, B. Herrera, Ignition delay and burning rate analysis of diesel–carbon nanotube blends stabilized by a surfactant: a droplet-scale study, Energies 16 (23) (2023) 7740.
[26] P. Kim, L. Shi, A. Majumdar, P. McEuen, Thermal transport measurements of individual multiwalled nanotubes, Phys. Rev. Lett. 87 (21) (2001) 215502.
[27] S. Berber, Y.K. Kwon, D. Tománek, Unusually high thermal conductivity of carbon nanotubes, Phys. Rev. Lett. 84 (20) (2000) 4613.
[28] K. Bashirnezhad, S. Bazri, M.R. Safaei, M. Goodarzi, M. Dahari, O. Mahian, A. S. Dalkılıça, S. Wongwises, Viscosity of nanofluids: a review of recent experimental studies, Int. Commun. Heat Mass Transf. 73 (2016) 114–123.
[29] V.Y. Rudyak, A.V. Minakov, M.I. Pryazhnikov, Preparation, characterization, and viscosity studding the single-walled carbon nanotube nanofluids, J. Mol. Liq. 329 (2021) 115517.
[30] S. Tanvir, L. Qiao, Surface tension of Nanofluid-type fuels containing suspended nanomaterials, Nanoscale Res. Lett. 7 (2012) 226.
[31] G. Singh, M. Esmaeilpour, A. Ratner, Investigation of combustion properties and soot deposits of various US crude oils, Energies 12 (12) (2019) 2368.
[32] G. Singh, M. Esmaeilpour, A. Ratner, The effect of acetylene black on droplet combustion and flame regime of petrodiesel and soy biodiesel, Fuel 246 (2019) 108–116.
[33] Yury Rodríguez-Yáñez, Daniel Bahena-Uribe, Bibiana Chávez-Munguía, Rebeca López-Marure, Stuart González-Monroy, Bulmaro Cisneros, Arnulfo Albores, Commercial single-walled carbon nanotubes effects in fibrinolysis of human umbilical vein endothelial cells, Toxicol. in Vitro 29 (2015) 1201–1214.
[34] L.M. Sargent, A.A. Shvedova, A.F. Hubbs, J.L. Salisbury, S.A. Benkovic, M. L. Kashon, D.T. Lowry, A.R. Murray, E.R. Kisin, S. Friend, K.T. McKinstry, L. Battelli, S.H. Reynolds, Induction of aneuploidy by single-walled carbon nanotubes, Environ. Mol. Mutagen. 50 (2009) 708–717.
[35] L. Guo, A. Von Dem Bussche, M. Buechner, A. Yan, A.B. Kane, R.H. Hurt, Adsorption of essential micronutrients by carbon nanotubes and the implications for nanotoxicity testing, Small 4 (2008) 721–727.
[36] S. Danczyk, B. Chehroudi, A. Ketsdever, G. Vaghjiani, A low power, novel ignition of fuels using Single-Wall Carbon Nanotubes (SWCNTs) and a camera flash, in: The Second Eglin Symposium on Nano Energetics Research, Engineering, and Education Facility, University of Florida, Shalimar, Florida, March .
[37] P.M. Ajayan, M. Terrones, A. de la Guardia, V. Hue, N. Grobert, B.Q. Wei, H. Lezec, G. Ramanath, T.W. Ebbesen, Nanotubes ignite with common flash, Science 296 (2002) 705.
[38] Chehroudi, B., Vaghjiani, G. L., Ketsdever, A., Method for distributed ignition of fuels by low-energy light sources, United States Patent Office, Patent Pending, 2004.
[39] B. Chehroudi, S.C. Danczyk, An innovative ignition method using SWCNTs and a camera flash, in: Nano Science and Technology Institute (NSTI), Nanotechnology Conference and Trade Show, Anaheim, California, May 8-12, 2005.